SPATIAL DENSITY ESTIMATION BASED SEGMENTATION OF SUPER-RESOLUTION LOCALIZATION MICROSCOPY IMAGES

Kuan-Chieh Jackie Chen[1,2,3]*, Ge Yang*[1,2]*, and Jelena Kovačević*[3,1,2]

[1]Dept. of Biomedical Eng., [2]Center for Bioimage Informatics, [3]Dept. of Electrical & Computer Eng.
Carnegie Mellon University, Pittsburgh, PA 15213, USA

ABSTRACT

Super-resolution localization microscopy (SRLM) is a new imaging modality that is capable of resolving cellular structures at nanometer resolution, providing unprecedented insight into biological processes. Each SRLM image is reconstructed from a time series of images of randomly activated fluorophores that are localized at nanometer resolution and represented by clusters of particles of varying spatial densities. SRLM images differ significantly from conventional fluorescence microscopy images because of fundamental differences in image formation. Currently, however, few quantitative image analysis techniques exist or have been developed or optimized specifically for SRLM images, which significantly limit accurate and reliable image analysis. This is especially the case for image segmentation, an essential operation for image analysis and understanding. In this study, we proposed a simple SRLM image segmentation technique based on estimating and smoothing spatial densities of fluorophores using an adaptive anisotropic kernel. Experimental results show that the proposed method provides robust and accurate segmentation of SRLM images and significantly outperforms conventional segmentation approaches such as active contour methods in segmentation accuracy.

***Index Terms*—** Super-resolution microscopy, STORM, fluorescence imaging, image segmentation, spatial density estimation

1. INTRODUCTION

Super-resolution microscopy techniques, which overcome the resolution limit of convention optical microscope by improving the resolution to $\sim$20 nm, are revolutionizing biological research with the ability to resolve biological structures at nanometer resolution. Super-resolution localization microscopy (SRLM) such as stochastic optical reconstruction microscopy (STORM) [1] and photo-activated localization microscopy (PALM) [2] achieve nanometer resolution by randomly activating separate fluorophores and computationally resolving their locations at nanometer resolution. The localized fluorophores from different raw image frames are combined into the final reconstructed image. While super-resolution techniques provide powerful tools for studying cellular processes at nanometer resolution, current analyses of SRLM imaging remain largely qualitative. SRLM images contain clusters of particles that reflect locations of individual activated fluorophores of varying spatial densities. Computational image analysis techniques that are developed or optimized specifically for the unique properties of SRLM images remain lacking.

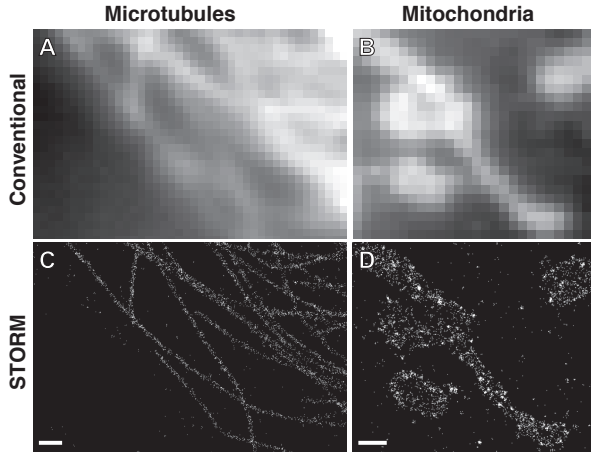

Fig. 1. Comparisons between conventional fluorescence microscopy and STORM images of microtubules and mitochondria. (A, C) Widefield and STORM images of microtubules, respectively; (B, D) widefield and STORM images of mitochondria, respectively. Scale bars, 500 nm.

Image segmentation is often the first step in quantitative image analysis. Although super-resolution images provide significantly improved spatial resolution in visualizing cellular structures (Fig. 1), this improvement in SRLM image analysis can only be achieved using reliable and accurate image segmentation tools.

In conventional epifluorescence or confocal microscopy images, objects can generally be characterized as continuous regions of fluorescence signals. In contrast, objects in SRLM images appear as clusters of estimated fluorophore locations

We thank Dr. Michael Davidson for providing the sample slide used to generate the data shown in Fig. 1. We gratefully acknowledge support from the US NSF through awards 1017278 (J.K.), and DBI-1149494, DBI-1052925, MCB-1052660 (G.Y).

with different spatial densities. To visualize detected fluorophores, common approaches are to render each particle as a normalized Gaussian kernel with the size proportional to the localization precision or to render a spatial histogram with a pre-specified bin size [3]. Direct segmentation of such images is problematic. As shown for example in Fig. 1, SRLM images appear punctate and the edges of image objects are often poorly defined due to random activation of fluorophores. Essentially, the randomly activated fluorophores provide a sampling of the underlying true spatial density distribution of all fluorophores.

Another commonly encountered issue in SRLM images is sparsely distributed artifacts (particles) appearing in the background regions, which may result from diffused fluorophores; these isolated features need to be properly addressed in image processing to avoid false segmentation. In general, reliable and accurate segmentation of SRLM images must take into account the unique properties of such images. An intuitive strategy is to estimate the underlying spatial density according to the sampled spatial distribution of the particles and then determine the criterion for segmenting the density image.

In this paper, we present a spatially adaptive density estimation based method for smoothing and segmenting super-resolution localization microscopy images. We propose to estimate local particle density using anisotropic kernels that adapt to local particle distributions. This kernel based method provides a way to connect separated particles in an object region as well as to interpolate object boundary without being misled by the random fluctuations of activated boundary fluorophores. Experimental results confirm the robustness and accuracy of the proposed method.

2. DENSITY ESTIMATION BASED SRLM IMAGE SEGMENTATION

Problem formulation To take into account the unique modality of SRLM images, we formulate the image segmentation problem as identifying different density regions from the spatial distribution of the particles. We propose a two-step process for SRLM image segmentation: 1) spatial density distribution estimation and 2) image segmentation based on thresholding that estimated density distribution. Inspired by previous work on density estimation [4], we start with a commonly adopted kernel density estimator, then follow by the proposed adaptive anisotropic kernel density estimator.

Density estimation with isotropic kernel Perhaps the most commonly used density estimator is the kernel density estimator. The idea is to estimate a continuous distribution from a finite set of points by placing a kernel centered at each of the points and taking the sum of all kernels. Kernel density estimation has been used previously in applications such as geographical information systems [5] and human motion tracking [6]

Specifically, suppose that we have a list of n points $x_1, x_2, \ldots, x_n$, sampled from some unknown density map f of a spatial area (in our application, the image). A classic 2D spatial kernel density estimator at location x is

$$\hat{f}(x) = \frac{1}{n}\sum_{i=1}^{n} K_i(x, x_i), \tag{1}$$

where K_i is a symmetric isotropic kernel function. We choose the Gaussian kernel, which is defined as

$$K_i(x, x') = \frac{1}{2\pi h^2}\exp\left(-\frac{||x - x'||^2}{2h^2}\right),$$

where h is a global spherical bandwidth, which can be estimated from the data by minimizing the L_2 risk function using cross-validation [4]. However, in SRLM images, h directly controls the resolution of the estimated density image as it represents the radius of the point-spread function of the density image. If the h is too small, the density estimator loses its power to connect the particles; if h is too large, the resolution degrades. Because the typical range of resolution for SRLM is $20 \sim 100$ nm [7], we choose h to be in the range of $10 \sim 50$ nm, i.e. half the resolution.

Density estimation with adaptive anisotropic kernel The main limitation of the isotropic kernel appears when it is placed at a location where the support of the underlying true density is close to one dimensional (for example, on the boundary). Isotropic kernel cannot properly represents the heterogeneity of the spatial density; it, instead, spreads its density mass equally along all spatial directions, thus, giving too much emphasis to background regions and too little along the boundary direction. This motivates us to use adaptive, anisotropic kernels for density estimation.

The adaptive anisotropic kernel density estimation associates with each point an anisotropic kernel. This kernel adapts to the local structure of the data points by estimating locally its scale, shape, and orientation. Again, the density function as in (1) at the location x is a sum of kernels centered at the surrounding points x_i where now each kernel $K_i(x, x_i)$ is the locally adaptive anisotropic Gaussian kernel

$$K_i(x, x_i) = \frac{1}{2\pi|\Sigma_i|}\exp\left(-\frac{1}{2}(x - x_i)^\top \Sigma_i^{-1}(x - x_i)\right),$$

where Σ_i is a positive definite covariance matrix that defines its configuration (scale, shape, and orientation).

To place the anisotropic kernel according to the spatial distribution of local data points, for the kernel located at the point x_i, we select its k-nearest neighbors x_1, $x_2, \ldots, x_k$, to estimate the covariance matrix

$$\Sigma_i = \frac{1}{k}\sum_{j=1}^{k}(x_j - x_i)(x_j - x_i)^\top.$$

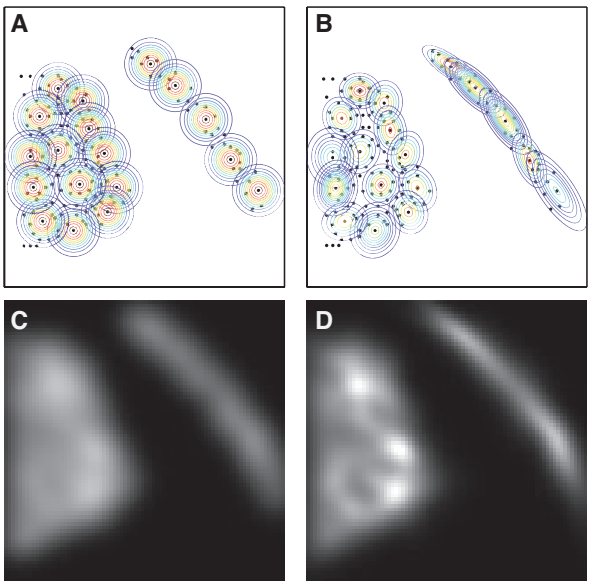

Fig. 2. Isotropic vs adaptive anisotropic kernels. Selected isotropic kernels (A) and adaptive anisotropic kernels (B) overlapped on the data points sampled from a curvilinear and a big blob structures. Estimated density images using isotropic kernels (C) and adaptive anisotropic kernels (D).

Here k must be at least $d+1$ to get the support of Σ_i, where $d=2$ is the spatial dimension. The size of the anisotropic kernel is controlled by the distance between x_k and x_i. Choosing a larger k helps to better estimate the distribution of local points; we must guard against too large a k, however, to prevent the resolution degradation. In this paper, we let k vary between 10 to 30.

Fig. 2 demonstrates the qualitative differences between the density estimations using isotropic kernel and adaptive anisotropic kernel. Estimating from the points sampled from two structures, the isotropic kernel yields a fair density estimation for both structures but generally spreads out the regions, making the region much bigger than the distribution of the points. In contrast, the adaptive anisotropic kernel follows the local distribution of the points and yields a density estimation with more precise boundaries compared to the one from the isotropic kernel.

Density threshold determination The estimated spatial density distribution provides a way of smoothing the SRLM images. This makes it possible to segment images by simple thresholding. We now need to determine a criterion to segment the regions with different density statistics. Here we assume two types of signals: signals of the actual fluorophores and background signals. We empirically model the density distribution of the foreground regions obtained by finding the non-zero density bins from the spatial histogram. The thresholding can then be set by finding the pth percentile of the densities. We found p to lie in the range of 1 to 15.

3. EXPERIMENTS AND RESULTS

We performed experiments on both simulated and real SRLM images of mitochondria and microtubules. The segmentation performance of the Chan-Vese active contour (AC) [8], the isotopic kernel density estimation based segmentation (IKDES), and the proposed adaptive anisotropic kernel density estimation based segmentation (AKDES) algorithms are compared qualitatively and quantitatively with the ground truth provided from simulated data.

Simulated data We simulated the fluorophore detections that are generated by SRLM imaging from given ground-truth. Two types of synthetic sample structures, microtubules and mitochondria, were produced to simulate common biological structures. Assuming a uniform fluorophore density in the object regions, we generated the detections of the activated fluorophores randomly with two different labeling densities of 1,000 and 2,000 detections in an image region of 2560×2560 nm, and added random artifacts in the background area with four different signal to artifact ratios of 5, 10, 20, and 40 dB.

Fig. 3 shows a qualitative comparison of the three segmentation algorithms. As previously noted, AC algorithm performs poorly on SRLM images. It is sensitive to local missing particle regions inside the object owing to the random fluctuations of the activated fluorophores in SRLM images. On the other hand, the IKDES method connects the region better but still suffers from over-segmentation and the false segmentation of the background artifacts. In contrast, the proposed AKDES method outperforms the other two methods in more precisely following the local boundary direction and being robust to fluctuations resulted from the random distribution of activated fluorophores, and thus provides more accurate segmentation in both sample structures. We have also tested graph-cut based segmentation methods [9] and found the performance to be inferior to the proposed method (data not shown).

For quantitative comparison, we use the following segmentation evaluation metrics: area similarity (AS) [10], which measures the goodness of segmentation compared to the ground truth, precision (P), which measures the ratio between the number of correctly segmented objects to the total number of segmented objects, and recall (R), which measures the ratio between the number of correctly segmented objects to the number of objects in the ground truth. Quantitative comparison is summarized in Table 1. All measures have been averaged over all objects and all images. From the results, both AC and IKDES methods perform poorly because of over-segmentation and false segmentation. In contrast, our proposed method outperforms the other two by a large margin (10-fold improvement). The area similarly results also show that the proposed method can correctly identify objects in both sample structures.

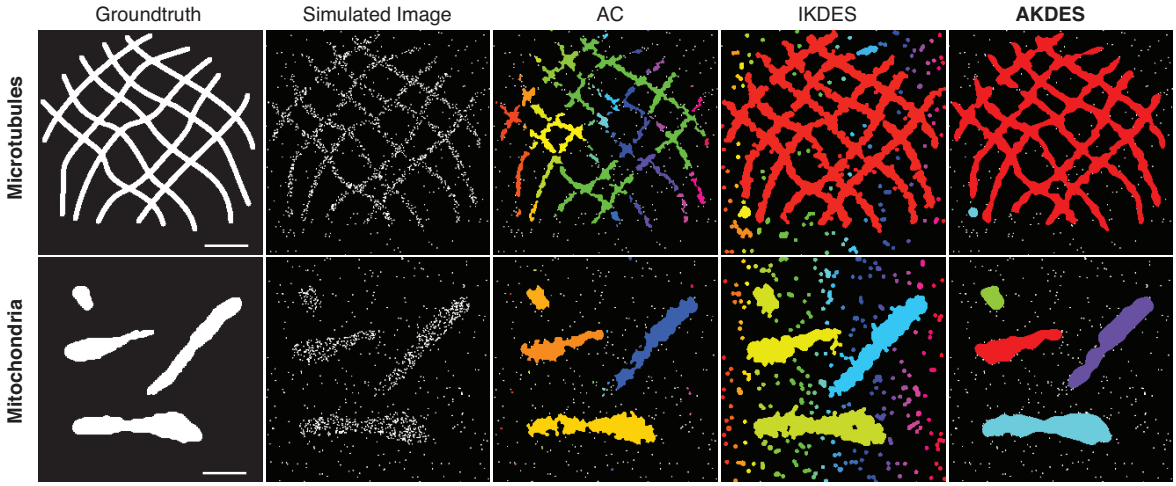

Fig. 3. Comparison of different image segmentation approaches on simulated images. The segmentation results are shown in random colors and overlapped on top of the simulated images. Scale bars, 500 nm.

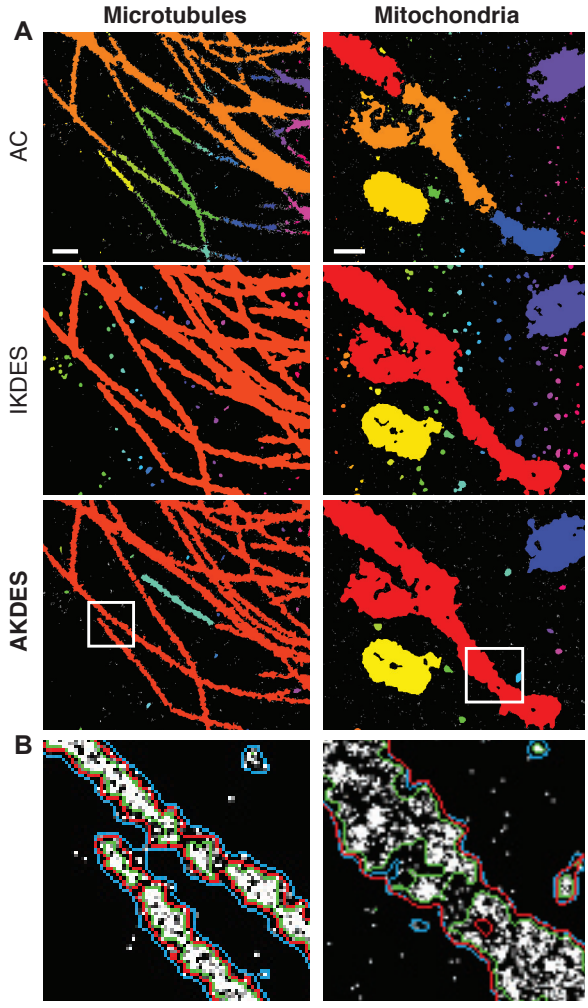

Fig. 4. Real SRLM image segmentation results. (A) Comparison of different image segmentation approaches. (B) Comparison of segmentation contours in regions corresponding to the boxed regions in A, where green, blue, and red contours refer to AC, IKDES, and AKDES results. Scale bars, 500 nm.

	Microtubules			Mitochondria		
	AC	IKDES	**AKDES**	AC	IKDES	**AKDES**
AS	0.64	0.75	**0.79**	0.90	0.88	**0.90**
P	0.01	0.02	0.37	0.31	0.44	**0.96**
R	1.00	1.00	1.00	1.00	1.00	1.00

Table 1. Quantitative comparison of segmentation results of simulated data.

SRLM data We further tested and compared these segmentation algorithms on real SRLM images of fluorescently labeled microtubules and mitochondria in fixed BS-C-1 cells imaged using a Nikon N-STORM system. Fig. 4 shows segmentation results in a region of $\sim$4,000$\times$4,000 nm. The AC method again only captures fragmented clusters of particles while the IKDES method suffers from over-segmentation and false segmentation of the background artifacts (see Fig. 4B). In contrast, our proposed method captures better the boundary of the objects and is more robust to the artifacts except for a few big clusters of particles in the background.

4. CONCLUSIONS

We presented a simple density estimation based approach for segmentation of super-resolution localization microscopy images. The proposed method uses an adaptive anisotropic kernel to estimate the underlying fluorophore density distribution, which can adjust the smoothing kernel according to the local spatial distribution. An empirically determined threshold is then used to segment the estimated density image. Experimental results show that, compared to active contour method that is sensitive to the random boundary fluctuations and isotropic kernel based method that suffers from over-segmentation, the proposed method provides more reliable and accurate segmentation.

5. REFERENCES

[1] M. J. Rust, M. Bates, and X. Zhuang, "Sub-diffraction-limit imaging by stochastic optical reconstruction microscopy (STORM)," *Nature Methods*, vol. 3, no. 10, pp. 793–795, 2006.

[2] E. Betzig, G. H. Patterson, R. Sougrat, O. W. Lindwasser, and et al., "Imaging intracellular fluorescent proteins at nanometer resolution.," *Science*, vol. 313, no. 5793, pp. 1642–5, 2006.

[3] D. Baddeley, M. B. Cannell, and C. Soeller, "Visualization of localization microscopy data.," *Microsc. Microanal.*, vol. 16, no. 1, pp. 64–72, Feb. 2010.

[4] D. W. Scott, Ed., *Multivariate Density Estimation*, Wiley Series in Probability and Statistics. John Wiley & Sons, Inc., Hoboken, NJ, USA, Aug. 1992.

[5] B. W. Silverman, *Density Estimation for Statistics and Data Analysis*, vol. 26, CRC press, 1986.

[6] T. Brox, B. Rosenhahn, D. Cremers, and H.-P. Seidel, "Non-parametric density estimation with adaptive, anisotropic kernels for human motion tracking," in *Proc. Second Workshop Human Motion*, 2007, pp. 152–165.

[7] L. Schermelleh, R. Heintzmann, and H. Leonhardt, "A guide to super-resolution fluorescence microscopy.," *J. Cell Biol.*, vol. 190, no. 2, pp. 165–175, July 2010.

[8] T. F. Chan and L. A. Vese, "Active contours without edges.," *IEEE Trans. Image Process.*, vol. 10, no. 2, pp. 266–277, Jan. 2001.

[9] Y. Boykov and V. Kolmogorov, "An experimental comparison of min-cut/max-flow algorithms for energy minimization in vision.," *IEEE Trans. Pattern Anal. Mach. Intell.*, vol. 26, no. 9, pp. 1124–1137, Sept. 2004.

[10] A. P. Zijdenbos, B. M. Dawant, R. A. Margolin, and A. C. Palmer, "Morphometric analysis of white matter lesions in MR images: Method and validation," *IEEE Trans. Med. Imag.*, vol. 13, pp. 716 – 724, Dec. 1994.